

Crystal field analysis of rare-earth ions energy levels in GaN



M. Stachowicz^{a,*}, A. Kozanecki^a, C.-G. Ma^{b,c}, M.G. Brik^b, J.Y. Lin^d, Hx Jiang^d, J.M. Zavada^e

^a Institute of Physics, Polish Academy of Sciences, 02-668 Warsaw, Poland

^b Institute of Physics, University of Tartu, Riia 142, Tartu 51014, Estonia

^c College of Mathematics and Physics, Chongqing University of Posts and Telecommunications, Chongqing 400065, PR China

^d Department of Electrical and Computer Engineering, Texas Tech University, Lubbock, TX 79409, USA

^e Department of Electrical and Computer Engineering, Polytechnic Institute of New York University, Brooklyn, NY 11201, USA

ARTICLE INFO

Article history:

Received 3 April 2014

Received in revised form 20 May 2014

Accepted 21 May 2014

Available online 14 June 2014

Keywords:

Impurity

Defect level

Condensed matter

Photoluminescence

Theoretical calculation

Local symmetry

ABSTRACT

Much effort has been put to achieve optoelectronic devices based on Er doped GaN, operating on the intra-4f-shell transitions of erbium. The key issue for good understanding of energy transfer mechanisms to Er and its luminescence properties is the position of Er³⁺ ions in the crystalline lattice of GaN. After doping, Er³⁺ ions are assumed to be placed in substitutional position for Ga³⁺ in GaN. Although Ga is positioned in high symmetry, tetrahedral [ErN₄]⁹⁻ cluster, deviations from this after doping are impossible to avoid because of a large difference in ionic radii of Ga³⁺ (47 pm) and Er³⁺ (89 pm). In this work we report on crystal field analysis of Er ion energy levels in cubic and hexagonal GaN. It is shown that local symmetry of Er in cubic GaN is D₂, whereas calculations reveal that in hexagonal GaN local symmetry is C_{3v}. Some trends in crystal field parameters of trivalent lanthanides in hexagonal GaN are discussed.

© 2014 Elsevier B.V. All rights reserved.

1. Introduction

Solid hosts doped with rare earth (RE) atoms has attracted attention in the last three decades due to the potential applications of RE-doped materials in optoelectronic semiconductor devices. Much of the research done on RE doping has focused on the erbium. Er³⁺ has sharp spectral emissions from the visible to near infrared region due to the intra-4f transitions. The transition from the first excited (⁴I_{13/2}) to the ground state (⁴I_{15/2}) at ~1.54 μm perfectly matches to the minimum loss window of silica fibers for optical communications. As it has been shown in many papers [1–4], strong thermal quenching of Er³⁺ luminescence at room temperature takes place in narrow band gap semiconductor hosts; it has been well established that the thermal stability of Er emission improves with an increased energy gap and better crystalline quality of the host. Furthermore, it has also been suggested that the environment created by more ionic hosts increases the emission efficiency of the intra-4f Er³⁺ transitions [2,5,6]. Therefore III-nitride wide band gap semiconductors appear to be the most appropriate host materials for Er ions, not only due to their structural and thermal stability, but also due to the recent advancements in growth techniques of high-quality samples. First attempts of incorporation of Er into GaN were through ion

implantation and reactive sputtering. Ion implantation damages lattice that has to be healed by post-implantation annealing. However, complete recovery of the implantation damage is difficult to achieve. Nowadays techniques for the doping of III-nitrides include *in situ* processes such as metal organic chemical vapor deposition (MOCVD) and molecular beam epitaxy (MBE). *In situ* incorporation of Er into semiconductors produces epilayers of high crystalline quality and improved Er-related emission in comparison to implanted samples. Using *in situ* incorporation techniques it is more probable to obtain the substitutional position of Er and therefore higher intensity of luminescence.

In the present paper we performed combined experimental and theoretical studies of the GaN:Er³⁺ samples, obtained by using MBE and MOCVD techniques. Detailed spectroscopic measurements of the highly resolved absorption and emission spectra of the samples were followed by the crystal field calculations of the Er³⁺ energy levels for two possible phases of GaN: cubic and hexagonal. The derived crystal field parameters allowed to calculate splitting of all the erbium levels and assign all the absorption peaks. Very good agreement with the experimental spectra was reached, with the root mean square (rms) deviation between the measured and calculated energy levels of about 13 cm⁻¹ only.

The structure of the paper is as follows: Section 2 deals with the experimental details, describing separately the samples preparation and spectroscopic measurements. Section 3 gives the details of the crystal field analysis and discussion of the comparison

* Corresponding author. Tel.: +48 228436601.

E-mail address: stachow@ifpan.edu.pl (M. Stachowicz).

between the experimental and calculated data. Section 4 offers a cross-cutting comparison of the crystal field effects for other lanthanides in GaN, which is based on the analysis of the archival literature data. Finally, the paper is concluded with a summary of the main results.

2. Experimental details and results

2.1. Experimental details

Samples used in this studies were cubic and hexagonal GaN:Er³⁺. The GaN samples with cubic symmetry were grown by MBE on GaAs substrate. After growth, the samples were implanted with Er ions at the energy of 300 keV to a dose of 10¹² cm⁻². The peak concentration of erbium in the implanted GaN was 10¹⁸ cm⁻³. After implantation the samples were annealed at 1000 °C in nitrogen gas flow.

In the case of hexagonal GaN:Er³⁺, the samples were uniformly doped across the layers with erbium to concentrations ranging from 2 × 10²⁰ cm⁻³ up to 2 × 10²¹ cm⁻³ during growth process by MOCVD on sapphire substrate. Details of the growth conditions of structures doped *in situ* were described in another paper [7].

The wide band gap of GaN allowed us to perform the site selective and photoluminescence excitation (PLE) measurements using a tunable Ti:sapphire laser pumped with an argon laser. The PL was also excited with other UV and visible lines of the Ar⁺ laser. The high-resolution PL spectra were detected using a Bomem DA3 Fourier Transform (FTIR) spectrometer equipped with a liquid-nitrogen cooled Ge detector. The spectral resolution of the FTIR spectrometer was 0.5 cm⁻¹. For PLE measurements a standard monochromator was used.

2.2. Experimental results

Measurements of the erbium ⁴I_{13/2} → ⁴I_{15/2} PL in cubic gallium nitride have been conducted within 6 K to 100 K temperature range using the FTIR spectrometer. Excitation was either with the 330 nm line of an Ar laser (non-resonant, over the band gap) or resonant to the ⁴I_{9/2} state. In the latter case the excitation wavelength was λ = 806.3 nm. Fig. 1 presents the PL spectra of Er³⁺ ions for over the band gap excitation at 330 nm. At 10 K a doublet of lines at 6513.4 and 6516.6 cm⁻¹ dominates the spectrum. Other doublet at 6467.1 and 6470.5 nm, whose intensity increase with

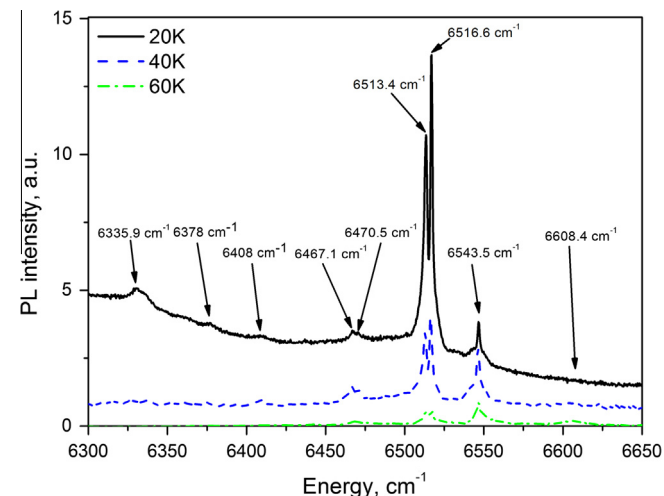


Fig. 1. PL spectra of Er³⁺ at over the band gap excitation with the 330 nm line of an Ar laser.

temperature relative to the dominant emission, can also be observed. Analysis of the spectra shows that relative intensities of some other lines increase too.

Fig. 2 presents the PL spectra of erbium in cubic GaN taken at 6 K, 30 K and 50 K at resonant excitation. Close similarity to the spectra in Fig. 1 can be noticed, however, the spectra in Fig. 2 reveal more distinct details, so these spectra are taken for further considerations.

In Fig. 2 one can distinguish the two characteristic regions of spectra. The high energy region contains the very intense and sharp spectral lines contrary to the low energy region, where broadened and weak lines are situated. Analyzing these spectra it was possible to find some regularities that have been organized in sets. As it can be noticed, the set of eight lines A1...A8 is noticeable at 6 K and the intensity of those decreases as temperature increases. Those lines are identified as transitions from the lowest level of the ⁴I_{13/2} excited state to levels of the ⁴I_{13/2} ground state, where lines marked as A6, A7 and A8 correspond to transitions to the lowest three levels of the ground state, which are in close energetic distance one to another. Maximum split of the ⁴I_{15/2} ground state is 185.4 cm⁻¹.

Much weaker lines B1...B8 can also be noticed at the temperature of liquid helium. As can be seen in spectra (Fig. 2), the intensity of those increases with temperature. This set of lines corresponds to transitions from the second level which is situated 30 cm⁻¹ above the lowest one of the ⁴I_{13/2} excited state to the ground state. Transitions from this energy level to energy levels of the lowest Γ_8 quartet are forbidden due to the parity, therefore the intensity is low. Third set of lines denoted as C1...C8, which refers to transitions from the third energy level of ⁴I_{13/2} excited state to the ground state, is easily noticeable at 50 K. The set of spectral lines denoted as C is shifted to higher energies, about 91.6 cm⁻¹, in comparison to set A. Please note that we are considering transitions of a single emitting Er³⁺ center. The spectra in Figs. 1 and 2 contain no trace of other competing Er-centers.

The identification, presented above, was the basis to propose the energy levels diagram for the ground ⁴I_{15/2} state and the first excited and the higher excited states of erbium in cubic GaN, taking into account the crystal field splittings of all J-manifolds.

In a cubic field the ⁴I_{9/2} state of free erbium ion splits into three sublevels – two quartets Γ_8 and doublet Γ_6 . Analyzing diagram presented in Fig. 2 some characteristic pattern of lines can be noticed. These are the close pairs of levels which are good candidates for Γ_8 quartets split into doublets by low symmetry component of the crystal field. It suggests that probably Er ion sits in cubic site symmetry with some distortion.

Only three out of five or seven levels, depending on symmetry, could have been distinguished in the ⁴I_{13/2} excited state. Unfortunately, we do not have any data for ⁴I_{11/2} excited state.

PLE spectra of Er³⁺ ions in cubic GaN were taken at 7 K and the detection wavelength was λ_{det} = 1534.4 nm, which is the most intense A8 spectral line in the PL spectra.

The PLE spectrum of Er³⁺ in cubic GaN, which is compared to Er³⁺ PLE spectra in hexagonal GaN in Fig. 3, allows us to notice differences in energies of transitions from the third excited to the ground states in both materials and to analyze and propose the energy levels scheme for the ⁴I_{9/2} excited state.

The identified spectra lines parameters are presented in Table 1. The lines enumerated from 1 to 5 in Table 1 correspond to energy levels of the ⁴I_{9/2} excited state in cubic GaN. In Fig. 3 we can see five lines among which there are two close pairs of levels suggesting distorted local cubic symmetry in agreement with the conclusion made for the ground state. One should remember that global symmetry stays the same, but local symmetry is disturbed due to the large difference between the ionic radii of the impurity (Er³⁺) ions and the host (Ga) ions.

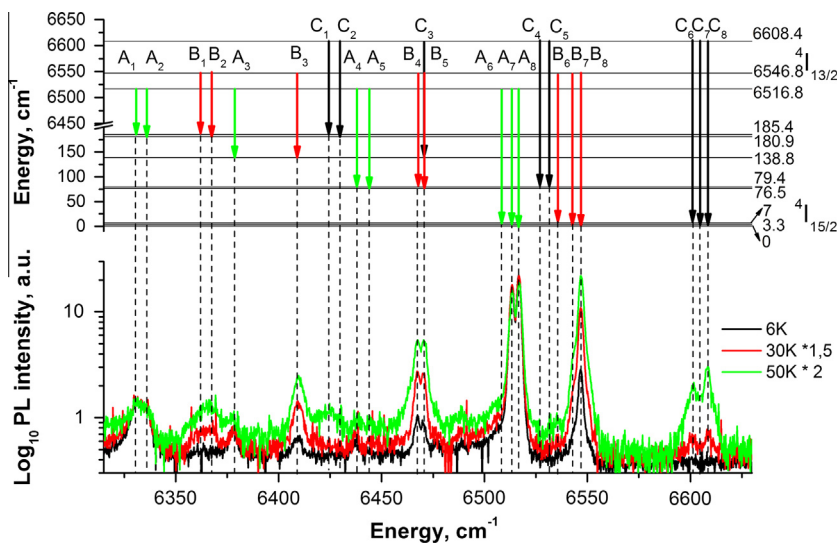


Fig. 2. PL spectra of Er³⁺ taken at 6 K, 30 K and 50 K and energy levels diagram of ground and first excited state of Er³⁺ in cubic GaN. Transitions from the excited to the ground state are connected to corresponding spectra lines with dotted lines.

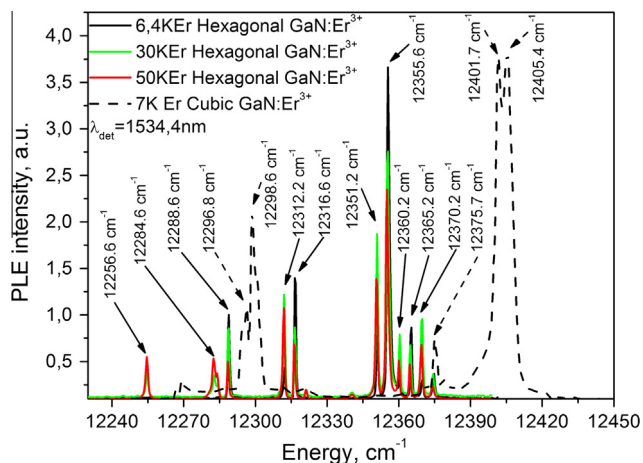


Fig. 3. Comparison of PLE spectrum of Er³⁺ in cubic GaN to PLE spectra of Er³⁺ in hexagonal GaN.

Table 1
⁴I_{15/2} → ⁴I_{9/2} spectral lines positions of Er³⁺ in cubic GaN (in cm⁻¹). The bold numbers denote ordinal number.

No.	Energy (cm ⁻¹)	No.	Energy (cm ⁻¹)	No.	Energy (cm ⁻¹)
1	12408,7	6	12405,4	11	12401,7
2	12405,3	7	12402,0	12	12398,3
3	12379,0	8	12375,7	13	12372,0
4	12301,9	9	12298,6	14	12294,9
5	12300,1	10	12296,8	15	12293,1

The very same methodology of experiments was used for Er³⁺ in hexagonal GaN as in the case of cubic GaN:Er.

Fig. 4a presents resonantly excited PL spectra of Er³⁺ in hexagonal GaN taken at 6 K, 40 K and 80 K using excitation wavelength λ_{exc} = 809.3 nm. The spectra contain 21 lines arranged in three sets. Energetic distance between sets A and B is ΔE₁ ≈ 9 cm⁻¹ and between sets B and C is ΔE₂ ≈ 19 cm⁻¹. On the basis of presented identification, the energy levels diagram was built for the first excited ⁴I_{13/2} and ground ⁴I_{15/2} state.

Later on, the PLE spectra have been recorded at 6 K and 50 K, at the detection wavelength of λ = 1534.4 nm, which is the most

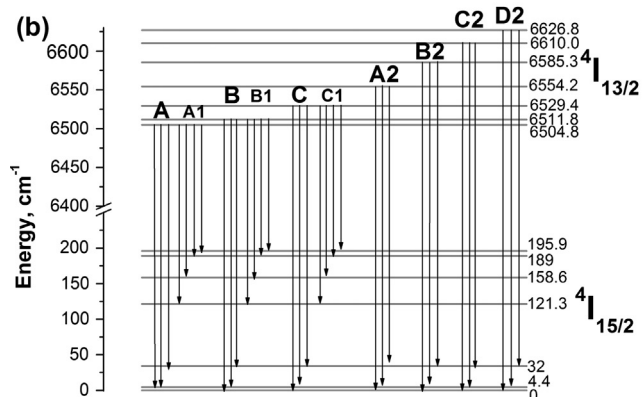
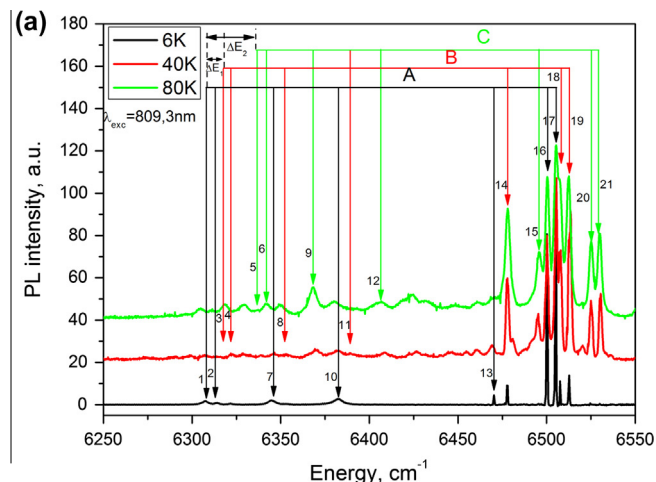


Fig. 4. (a) Resonantly excited spectra of Er³⁺ in hexagonal GaN taken at 6 K, 40 K and 80 K and (b) energy levels scheme of Er³⁺ in hexagonal GaN for the ground and first excited state.

intense (18) spectral line in the PL spectra (see Fig. 3). As it can be seen, only the intensity of lines changes with temperature as in the case of Er³⁺ in cubic GaN.

Employing the same methodology of identification and analysis as in the case of ⁴I_{13/2} excited state of Er³⁺, the energy levels of the

next $^4I_{11/2}$ and $^4I_{9/2}$ excited states were identified and energy levels schemes were proposed.

Taking closer look at the energy levels schemes (Figs. 4b and 5), it can be noticed that we were able to identify seven out of eight levels in the ground state and virtually all levels of excited states. As it was shown by Makarova et al. [18], only one dominant emitting erbium center could be distinguished in MOCVD grown GaN:Er³⁺ thin films. Considering the number of levels in each state we assume that the C_{3v} point-group is the closest symmetry to the observed situation.

Possessing this unique set of spectroscopic data about Stark's splits and energy levels positions in each state, it is possible to conduct theoretical crystal field (CF) analysis and calculations of Er³⁺ ions in both material, which will support and further strengthen the experimental results.

3. Modeling of energy levels for $4f^{11}$ configuration of Er³⁺ in GaN

3.1. Crystal structure of hexagonal and cubic GaN

Two structural modification of GaN considered in the present paper, are the hexagonal wurtzite (WZ) and cubic zinc blende types. The first one crystallizes in the P63mc space group (No. 186), whereas the second one – in the cubic space group F-43m (No. 216). The unit cells of both structures are shown in Fig. 6.

The usual crystal structure of GaN is the hexagonal wurtzite (WZ) type, which has nearly the same tetrahedral nearest-neighbor atomic coordination as cubic zinc blende (ZB) type structure. WZ lattice constants a and c have relation as $c/a = \sqrt{\frac{8}{3}} = 1.633$ and internal parameter $u = 3/8 = 0.375$, where uc corresponds to the length of the bonds parallel to [0001].

In the WZ structure, however, there are pairs of cation (Ga³⁺ or Er³⁺ in the case of substitutional doping) and anion (N⁻) attracted

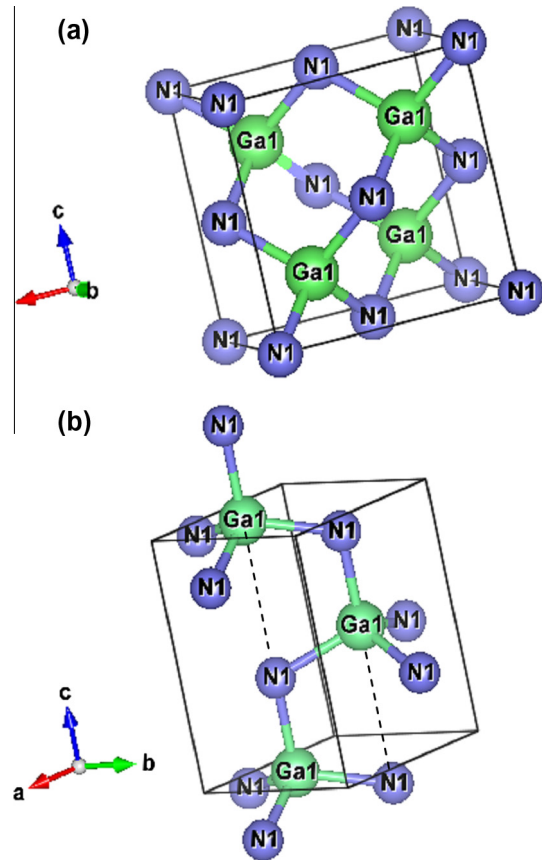


Fig. 6. Graphical representation of unit cell of (a) cubic and (b) hexagonal GaN. Drawn with VESTA [10].

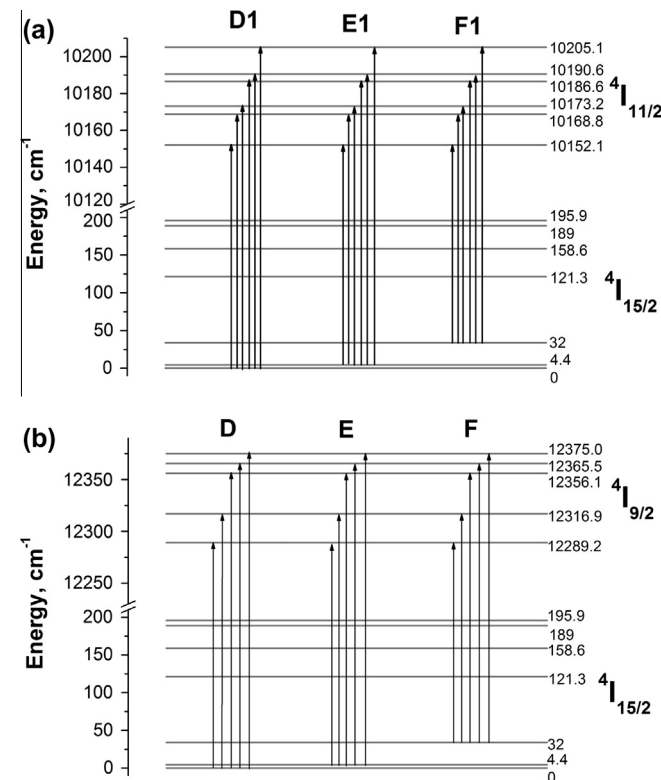


Fig. 5. Energy levels diagrams of Er³⁺ in hexagonal GaN of: (a) the second $^4I_{11/2}$ excited state and (b) the third $^4I_{9/2}$ excited state.

to each other by electrostatic force. It is considered that these electrostatic interactions make WZ–GaN more stable than ZB – GaN because ionicity of these compounds is large among the III–V compound semiconductors.

Although the nearest Ga (or Er after doping) environment is almost the same in both phases, there exists a certain difference in the bond lengths and angles between the bonds. Thus, in the hexagonal phase the Ga – N bonds are (all in Å): 1.94588 (parallel to the c axis) and 1.95263 ($\times 3$) [8], whereas in the cubic phase those bonds are all equal to 1.93124 [9].

All the N–Ga–N angles in the cubic phase are equal then to 109.47°. Those angles in the hexagonal phase are 109.40°, if the Ga–N bond is parallel to the c axis and 109.54°, otherwise.

This consideration of the GaN crystal structures allows to conclude that the point symmetry of the Er³⁺ impurity center in the hexagonal phase should be lower than in the cubic one.

3.2. Theoretical background

The standard form of the Hamiltonian acting within the $4f^N$ configuration of trivalent lanthanide (Ln³⁺) ions in any host can be commonly written as [11–13]:

$$\begin{aligned}
 H = E_{avg} + \sum_{k=2,4,6} F^k f_k + \zeta_{4f} A_{so} + \alpha L(L+1) + \beta G(G_2) + \gamma G(R_7) \\
 + \sum_{i=2,3,4,6,7,8} T^i t_i + \sum_{h=0,2,4} M^h m_h + \sum_{k=2,4,6} P^k p_k + \sum_{k,q} B_q^k C_q^{(k)}
 \end{aligned}
 \quad (1)$$

where the italic and bold letters represent the parameters and operators, respectively. The first term E_{avg} is the barycenter of the $4f^N$

electronic configuration. The second and the third terms describe the Coulomb and spin-orbit (SO) interactions and produce the set of the free ion $2^{S+1}L_J$ multiplets. The next four terms are the effective two- and three- electron Coulomb correlation contributions from higher configuration with the same parity. The two-body magnetically correlated interactions described by the Marvin integrals M^h represent the spin-spin and spin-other-orbit relativistic corrections; electrostatically correlated SO contributions are the two-body interactions represented by the P^k entries. Following Carnall et al. [12], the ratios of M^k ($k=2$ and 4) to M^0 and P^k ($k=4$ and 6) to P^2 are usually constrained to minimize the number of fitting parameters. For the $4f^N$ and $4f^{14-N}$ configurations ($N \leq 7$), the two- and three- body parameters exist only if $N > 1$ and $N > 2$ in the above equation. All the terms mentioned above represent the “free-ion” Hamiltonian, whose parameters vary slightly from one host to another due to nephelauxetic effect [14]. The last term describes the anisotropic components of the crystal field (CF) interactions; the B_q^k entries are referred to as the crystal field parameters (CFPs), and $C_q^{(k)}$ are the spherical operators (here the Wybourne notation is adopted [13]). There can be in general up to 27 different CFPs, many of which can be equal to zero. The number of non-zero CFPs depends upon the local site symmetry of the position occupied by the rare earth ion and considerably decreases when going to the sites of higher symmetry.

The site symmetry of the implanted Ln^{3+} ions in GaN is always dependent on the different growth and annealing conditions that are used. As described in the experimental sections of Refs. [15–19], the GaN:Er $^{3+}$ layers with the different phases (i.e. the cubic and hexagonal phases) can be obtained by respectively employing the Molecular Beam Epitaxy and metal-organic chemical vapor deposition (MOCVD). For the cubic and hexagonal GaN:Ln $^{3+}$, Ln $^{3+}$ ions are respectively incorporated into the substitutional Ga sites with the tetrahedral and hexagonal site symmetry, i.e. D_2 and C_{3v} , as reported in Refs. [20–25].

Since the configuration interaction parameters (α , β and γ) and other small correction parameters (T^l , M^0 and P^2) are less sensitive to the host CF environment than the Coulomb and SO coupling parameters (F^k and ζ_{4f}), the former can be regarded as the constants directly taken from Ref. [12]. To further minimize the number of the fitting parameters, the ratios of electrostatic Coulomb parameters F^4 and F^6 to F^2 are also constrained, and fixed as those ratios from Ref. [12]. The CFPs, Slater parameters F^2 , spin-orbit coupling parameter ζ_{4f} and the configuration barycenter parameter E_{avg} can be freely varied to obtain the ultimate optimization results. All the fitting calculations below employed the f-shell programs written by M.F. Reid.

3.3. Energy level calculation for the cubic GaN:Er $^{3+}$

For the cubic GaN:Er $^{3+}$, the CF splittings of the ground $^4I_{15/2}$, and excited $^4I_{13/2}$ and $^4I_{9/2}$ multiplets have been fairly well measured in Refs. [23,24]; the corresponding energy level data can be also found in Table 2. While Ref. [23] treats about crystal field calculation of Tb $^{3+}$ in GaN, the symmetry properties of the Tb $^{3+}$ should be the same as those of Er $^{3+}$ center, so we used the idea of considering the D_2 and D_{2d} symmetries. The relevant CF fitting work has been preliminarily made by Glukhanyuk et al. [17]. However, their CF fitting was not built upon all the observed data, but only on the CF energy levels of $^4I_{9/2}$ multiplet. Moreover, they adopted the relatively high D_{2d} point group as the site symmetry of Er $^{3+}$ ion in the cubic GaN, but this seems to not agree with the case of lower site symmetry and larger crystal lattice distortion after doping due to a large difference in ionic radii of Ga $^{3+}$ (47 pm) and Er $^{3+}$ (89 pm) [26]. Therefore, it is necessary to re-fit these data employing the appropriate site symmetry.

The site symmetry of an impurity ion position after the crystal lattice relaxation is possibly a direct or indirect subgroup of the “parent” site symmetry before doping. We chose the D_2 point-group as the suitable site symmetry to fit the experimental data based on the following three considerations. First, the D_2 point group describes a lower symmetry than D_{2d} , which will increase the number of CFPs and possibly improve the fitting’s quality, as will be shown below. Second, it is the indirect subgroup of the “parent” T_d group, which leads to the conclusion that the [ErN $_4$] $^{9-}$ cluster in the cubic phase will be strongly distorted. Third, the present choice is consistent with the site assignments of GaN:Tb $^{3+}$ made by Gruber et al. [23]. In the following, two CF fitting calculations respectively adopting D_{2d} and D_2 site symmetries are described to show the rationality of the above choice.

The CF Hamiltonian in the case of a CF of D_{2d} symmetry is:

$$\mathbf{H}_{CF} = B_0^2 C_0^{(2)} + B_0^4 C_0^{(4)} + B_4^4 (C_4^{(4)} + C_{-4}^{(4)}) + B_0^6 C_0^{(6)} + B_4^6 (C_4^{(6)} + C_{-4}^{(6)}) \quad (2)$$

If the D_2 symmetry is further employed, some additional terms will appear in the Hamiltonian:

$$\mathbf{H}_{CF} = B_0^2 C_0^{(2)} + B_2^2 (C_2^{(2)} + C_{-2}^{(2)}) + B_0^4 C_0^{(4)} + B_2^4 (C_2^{(4)} + C_{-2}^{(4)}) + B_4^4 (C_4^{(4)} + C_{-4}^{(4)}) + B_0^6 C_0^{(6)} + B_2^6 (C_2^{(6)} + C_{-2}^{(6)}) + B_4^6 (C_4^{(6)} + C_{-4}^{(6)}) + B_6^6 (C_6^{(6)} + C_{-6}^{(6)}) \quad (3)$$

where all CFPs are real. All the fitting parameters were obtained and summarized in Table 3, whereas the calculated energy level values were also collected in Table 2. Agreement between the calculated and observed CF energy levels of the cubic GaN:Er $^{3+}$ can be characterized by the standard root-mean-square deviation, whose values for these two symmetries (i.e. D_{2d} and D_2) are respectively 20.8 and 16.6 cm^{-1} . It may be argued that the improvement is not very large (due to the increase of the CFP number), but the energy differences between the calculated and experimental energy levels have been greatly minimized about from 20 to 10 cm^{-1} after the site symmetry is further lowered (from D_{2d} to D_2). Moreover, agreement between the barycenters of the calculated and observed energy levels is much improved if the D_2 symmetry is employed. All these considerations confirm that Er $^{3+}$ ions in the cubic GaN could be situated at the greatly distorted site with the D_2 point-group symmetry. Calculated values for both symmetries D_2 and D_{2d} are compared to experimental data in form of energy levels diagrams, which are presented in Fig. 7.

3.4. Energy level calculation for the hexagonal GaN:Er $^{3+}$

The energy level diagram including four lowest multiplets of Er $^{3+}$ ion ($^4I_{15/2}$, $^4I_{13/2}$, $^4I_{11/2}$ and $^4I_{9/2}$) in the hexagonal GaN can be easily established according to the previously measured data of Makarova and Glukhanyuk et al. [18,19]. The new CF splitting data were obtained by re-measuring the original spectra; the new data are listed in Table 2, whereas the original data for CF energy levels [19] were also collected as a comparison. In addition to the early experimental work for the hexagonal GaN:Er $^{3+}$, the theoretical energy level analysis based on them was also carried out by Maâlej et al. [24], but they employed the free-ion energy level diagram plotted by Steckl et al. [25]. Actually, the data of Steckl et al. are based on the emission spectrum of free trivalent Er $^{3+}$ ion given by Dieke and Crosswhite, and thus are not directly suitable to be used for an analysis of the CF energy levels. This is just the reason why some of the three-body parameters in Ref. [24] are too large to be accepted. Therefore, in the following, we re-carried out a

Table 2
Measured and calculated energy levels (in cm^{-1}) of Er^{3+} ions respectively in the cubic and hexagonal GaN.

Multiplets	Level no.	Cubic GaN:Er ³⁺					Hexagonal GaN:Er ³⁺				
		E_{exp}	D_2 symmetry		D_{2d} symmetry		$E_{\text{exp}}(\text{old})$	$E_{\text{exp}}(\text{new})$	C_{3v} symmetry		
			E_{calc}	$\Delta = E_{\text{exp}} - E_{\text{calc}}$	E_{calc}	$\Delta = E_{\text{exp}} - E_{\text{calc}}$			E_{calc}	$\Delta = E_{\text{exp}}(\text{new}) - E_{\text{calc}}$	
⁴ I _{15/2}	1	0.0	0.2	-0.2	-21.1	21.1	0	0	4.7	-4.7	
	2	3.3	5.3	-2.0	17.4	-14.1	4.5	4.4	10.2	-5.8	
	3	7.0	17.5	-10.5	25.9	-18.9	33.9	32.0	39.1	-7.1	
	4	76.5	63.4	13.5	84.2	-7.7	121.3	121.3	111.0	10.3	
	5	79.4	88.4	-9.0	86.3	-6.9	158.6	158.6	150.8	7.8	
	6	138.8	134.8	4.0	136.3	2.5	-	-	166.3	-	
	7	180.9	170.4	10.5	157.9	23.0	189.0	189.0	184.3	4.7	
	8	185.4	192.2	-6.8	184.2	1.2	195.9	195.9	195.5	0.4	
⁴ I _{13/2}	9	6516.8	6513.0	3.8	6526.6	-9.8	6504.8	6504.8	6510.1	-5.3	
	10	-	6526.3	-	6538.6	-	6511.8	6511.8	6515.5	-3.7	
	11	6546.8	6547.7	-0.9	6550.3	-3.5	6529.4	6529.4	6543.2	-13.8	
	12	-	6552.3	-	6566.8	-	-	-	6602.1	-	
	13	-	6583.5	-	6571.0	-	-	-	6613.3	-	
	14	6608.4	6614.0	-5.6	6595.5	12.9	-	-	6633.8	-	
	15	-	6628.6	-	6603.5	-	-	-	6651.6	-	
⁴ I _{11/2}	16	-	10141.9	-	10161.2	-	10115.6	10152.1	10137.0	15.1	
	17	-	10154.8	-	10163.2	-	10132.9	10168.8	10150.2	18.6	
	18	-	10163.4	-	10167.6	-	10138.7	10173.2	10165.2	8.0	
	19	-	10179.8	-	10177.2	-	10150.5	10186.6	10186.9	-0.3	
	20	-	10198.6	-	10179.5	-	10153.0	10190.6	10201.2	-10.6	
	21	-	10207.9	-	10189.5	-	10168.1	10205.1	10212.2	-7.1	
⁴ I _{9/2}	22	12300.1	12284.9	15.2	12285.8	14.3	12288.6	12288.6	12277.5	11.1	
	23	12301.9	12315.8	-13.9	12311.3	-9.4	12316.6	12316.6	12321.6	-5.0	
	24	12379.0	12378.3	0.7	12363.6	15.4	12355.6	12355.6	12340.3	15.3	
	25	12405.3	12397.7	7.6	12395.4	9.9	12365.2	12365.2	12376.0	-10.8	
	26	12408.7	12414.1	-5.4	12438.7	-30.0	12374.6	12374.6	12391.6	-17.0	
⁴ F _{9/2}	27	-	15147.6	-	15169.9	-	-	-	15106.6	-	
	28	-	15160.5	-	15171.4	-	-	-	15123.4	-	
	29	-	15178.7	-	15179.7	-	-	-	15135.6	-	
	30	-	15190.2	-	15196.2	-	-	-	15184.0	-	
	31	-	15244.1	-	15210.4	-	-	-	15228.5	-	

Note: The stand deviations for three calculated cases, i.e. D_{2d} , D_2 and C_{3v} , are respectively 20.8, 16.6 and 13.3 cm^{-1} .

Table 3
The optimized Hamiltonian parameters (in cm^{-1}) for Er^{3+} ions respectively in the cubic and hexagonal GaN and Nd^{3+} ions in the hexagonal GaN.

Parameter	Cubic GaN:Er ³⁺		Hexagonal GaN:Er ³⁺	Hexagonal GaN:Nd ³⁺
	D_{2d} symmetry	D_2 symmetry	C_{3v} symmetry	C_{3v} symmetry
E_{avg}	35364.6	35362.2	35255.1	23225.3
F^2	96235.2	96215.7	95767.3	68936.3
ζ_{4f}	2373.3	2373.9	2370.3	868.9
B_0^2	-43.3	166.8	-300.5	-382.9
B_2^2	-	-249.9	-	-
B_0^4	-150.2	456.8	921.4	24.4
B_2^4	-	-145.6	-	-
B_3^4	-	-	533.7	-1540.3
B_4^4	-68.1	23.6	-	-
B_0^6	412.7	-190.0	126.2	-314.3
B_2^6	-	-252.1	-	-
B_3^6	-	-	-0.8	-229.0
B_4^6	264.8	-53.7	-	-
B_6^6	-	-162.7	-23.3	-408.2
N_E	16	16	21	20
N_p	8	12	9	9
σ	20.8	16.6	13.3	29.5

Notes: The ratios of F^4 and F^6 to F^2 and other free-ion parameter values not indicated here were fixed at the values given in Ref. [12]. N_E and N_p are the numbers of experimental levels fitted and the numbers of freely-adjustable parameters. The standard root-mean-square deviation σ was defined as:

$$\sigma = \sqrt{\sum_{i=1, \dots, N_E} (E_i(\text{calc.}) - E_i(\text{exp.}))^2 / (N_E - N_p)}$$

where $E_i(\text{calc.})$ and $E_i(\text{exp.})$ are respectively the theoretical and measured CF energy level values.

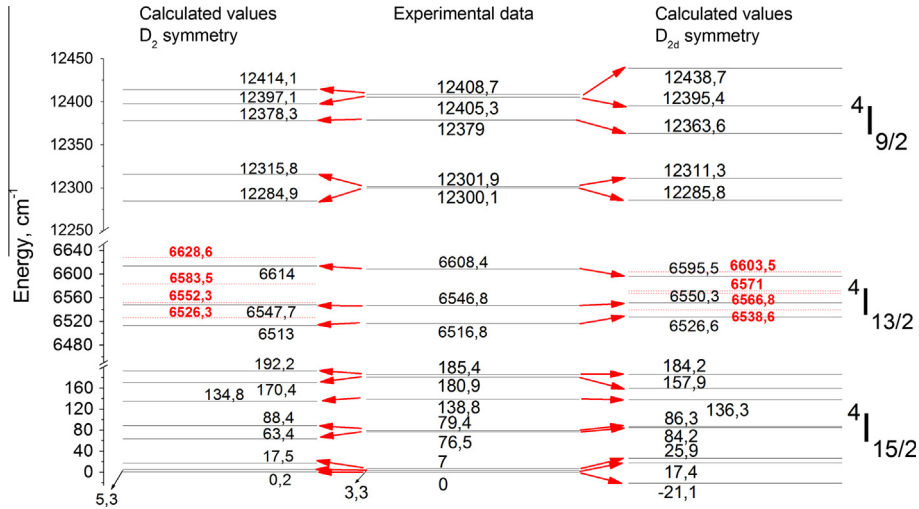


Fig. 7. Experimental energy levels scheme of ⁴I_{15/2}, ⁴I_{13/2} and ⁴I_{9/2} states of Er³⁺ in cubic GaN compared to calculated values for both symmetries. Dashed red lines are not observed in experimental spectra. (For interpretation of the references to color in this figure legend, the reader is referred to the web version of this article.)

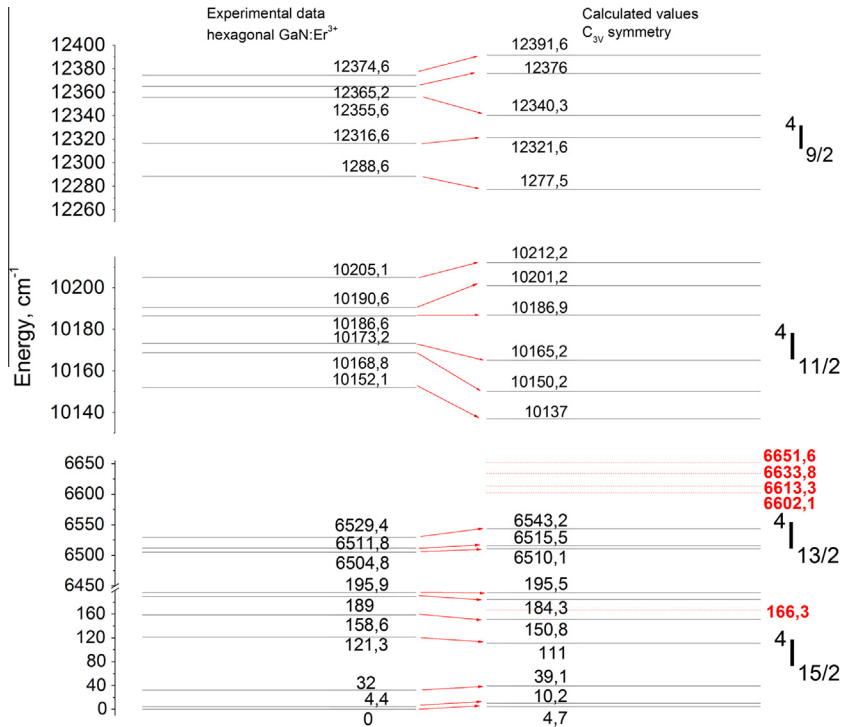


Fig. 8. Comparison of experimental data to re-fixed theoretical values of ground first three excited states of Er³⁺ in hexagonal GaN. Dotted red lines are not observed in experimental spectra. (For interpretation of the references to color in this figure legend, the reader is referred to the web version of this article.)

theoretical study based on the updated energy levels of the hexagonal GaN:Er³⁺.

The parameterized CF Hamiltonian of 4f¹¹ configuration of Er³⁺ ions with C_{3v} site symmetry may be expressed as follows:

$$\begin{aligned}
 H_{cf} = & B_0^2 C_0^{(2)} + B_0^4 C_0^{(4)} + B_3^4 (C_{-3}^{(4)} - C_3^{(4)}) \\
 & + B_0^6 C_0^{(6)} + B_3^6 (C_{-3}^{(6)} - C_3^{(6)}) + B_6^6 (C_6^{(6)} + C_{-6}^{(6)})
 \end{aligned}
 \tag{4}$$

where all CFPs are real. By following the mentioned fitting scheme in combination with the Eq. (4), F², E_{avg} and six CFPs were obtained and summarized in Table 3, whereas the calculated energy level

values were collected in Table 2 to show the consistency with the experimental data. Fig. 8 presents energy levels schemes of the calculated and experimental values for better understanding. The standard root-mean-square deviation is 13.3 cm⁻¹. Another interesting problem is how to evaluate the deviation level from the T_d symmetry for the present local structure. In the following, we describe one method using the point-group basis to expand CF Hamiltonian to understand the deviation level from the “parent” symmetry.

The group chain was firstly chosen as SU₂ ⊃ T_d ⊃ C_{3v} according to the site symmetry of the substituting Er³⁺ ions in the hexagonal GaN. Thus, by referring to the table of the unitary conversion

coefficients between the bases with different group chains in the Ref. [27], the CF Hamiltonian of Er^{3+} ions with C_{3v} site symmetry can be re-expressed as follows:

$$\mathbf{H}_{\text{cf}} = B_C^4 \left[\frac{\sqrt{7}}{3\sqrt{3}} C_0^{(4)} - \frac{\sqrt{10}}{3\sqrt{3}} (C_{-3}^{(4)} - C_3^{(4)}) \right] + B_C^6 \left[\frac{4\sqrt{2}}{9} C_0^{(6)} + \frac{\sqrt{35}}{9\sqrt{3}} (C_{-3}^{(4)} - C_3^{(4)}) + \frac{\sqrt{77}}{9\sqrt{6}} (C_6^{(6)} + C_{-6}^{(6)}) \right] \quad (5a)$$

$$+ B_D^2 C_0^{(2)} + B_D^4 \left[\frac{2\sqrt{5}}{3\sqrt{3}} C_0^{(4)} + \frac{\sqrt{7}}{3\sqrt{6}} (C_{-3}^{(4)} - C_3^{(4)}) \right] + B_D^6 \left[\frac{\sqrt{11}}{\sqrt{42}} (C_{-3}^{(6)} - C_3^{(6)}) - \frac{\sqrt{5}}{\sqrt{21}} B_6^6 (C_6^{(6)} + C_{-6}^{(6)}) \right] \quad (5b)$$

$$+ B_D^6 \left[\frac{7}{9} C_0^{(6)} - \frac{4\sqrt{10}}{9\sqrt{21}} (C_{-3}^{(4)} - C_3^{(4)}) - \frac{4\sqrt{11}}{9\sqrt{21}} (C_6^{(6)} + C_{-6}^{(6)}) \right] \quad (5c)$$

where B_C^6 , B_D^2 , B_D^4 , B_D^6 and $B_D^{6'}$ are the newly-defined CFPs under point-group basis, and their number still keeps invariant, i.e. 6. Here Eq. (5a) shows the CF part with the cubic symmetry described by two cubic CFPs marked with the subscript “C”. The last two Eqs. (5b) and (5c) are the additional appearing terms due to the symmetry descent from T_d to C_{3v} , where four CFPs with the subscript “D” are used to reflect the distortion. The six newly-defined CFPs can be connected with the old CFPs defined by Wybourne [13] by using the following conversion relations:

$$\begin{aligned} B_0^2 &= B_D^2 \\ B_0^4 &= \frac{\sqrt{7}}{3\sqrt{3}} B_C^4 + \frac{2\sqrt{5}}{3\sqrt{3}} B_D^4 \\ B_3^4 &= -\frac{\sqrt{10}}{3\sqrt{3}} B_C^4 + \frac{\sqrt{7}}{3\sqrt{6}} B_D^4 \\ B_0^6 &= \frac{4\sqrt{2}}{9} B_C^6 + \frac{7}{9} B_D^{6'} \\ B_3^6 &= \frac{\sqrt{35}}{9\sqrt{3}} B_C^6 + \frac{\sqrt{11}}{\sqrt{42}} B_D^6 - \frac{4\sqrt{10}}{9\sqrt{21}} B_D^{6'} \\ B_6^6 &= \frac{\sqrt{77}}{9\sqrt{6}} B_C^6 - \frac{\sqrt{5}}{\sqrt{21}} B_D^6 - \frac{4\sqrt{11}}{9\sqrt{21}} B_D^{6'} \end{aligned} \quad (6)$$

By applying the above relation to the optimized CFPs listed in Table 2, the CFPs under point-group basis for the hexagonal GaN:Er^{3+} can be easily evaluated and listed in Table 4.

Table 4
The CFPs under point-group basis, the CF invariant S and its cubic and non-cubic components S_C and S_D , and the deviation level from T_d symmetry P for the hexagonal GaN:Ln^{3+} ($\text{Ln} = \text{Pr, Nd, Sm, Er}$ and Yb) (unit: cm^{-1}).

Hexagonal GaN:Ln^{3+}	Pr^{3+}	Nd^{3+}	Sm^{3+}	Er^{3+}	Yb^{3+}
B_D^2	−46.5	−382.9	−48.9	−300.5	−96.0
B_C^4	792.0	1887.2	−46.4	−180.4	575.9
B_D^4	−1499.8	−1088.1	−972.6	1177.3	−698.6
B_C^6	1054.2	−696.3	442.1	60.2	556.5
B_D^6	−1502.7	164.0	−527.4	21.9	−528.7
$B_D^{6'}$	910.8	158.62	533.3	113.6	455.4
S_C	1396.5	2332.7	438.1	221.3	873.2
S_D	2520.4	1439.5	1436.2	1474.9	1084.1
S	2476.0	2741.1	1511.1	1491.4	1392
P	49.13%	85.10%	30.51%	14.84%	62.73%

Notes: The CFPs under point-group basis are defined according to Eqs. (5a), (5b), (5c), and their values can be evaluated by using the conversion relation with the traditional CFPs defined by Wybourne [13] i.e. Eq. (6) and the obtained CFPs in Table 2 and Refs. [20,22,25]. The cubic and non-cubic components S_C and S_D of the CF invariant S can be given by employing Eq. (7), and S is equal to $(S_C^2 + S_D^2)^{1/2}$. The deviation level from T_d symmetry P is defined as S_C/S .

The direct comparison of the cubic CFPs with those distorted ones cannot characterize the deviation level from T_d symmetry. The CF invariant is a good parameter providing a good way of comparing the CF influence imposed by the different coordination environments [28]. Thus, we proposed two CF strength parameters respectively standing for the cubic and non-cubic components as shown below:

$$S_C = \sqrt{\frac{4\pi}{9} (B_C^4)^2 + \frac{4\pi}{13} (B_C^6)^2} \quad (7)$$

$$S_D = \sqrt{\frac{4\pi}{5} (B_D^2)^2 + \frac{4\pi}{9} (B_D^4)^2 + \frac{4\pi}{13} [(B_D^6)^2 + (B_D^{6'})^2]}$$

where the subscripts “C” and “D” have the same meanings with those in CFPs. It is easily deduced that $S = (S_C^2 + S_D^2)^{1/2}$ is the total CF strength parameter, and must be equal to the value obtained from the formula of Auzel et al. [28] due to the unitarity of the present point-group transformations. The deviation level from T_d symmetry can be described by the ratio $P = S_C/S$. If P is very close to unit one, that means the distortion is very small; otherwise, there is a much bigger deviation. For the hexagonal GaN:Er^{3+} , the total CF invariant and P values are easily obtained and listed in Table 4. The small P value for the hexagonal GaN:Er^{3+} (14.84%) shows the coordination environment of Er^{3+} doped in the hexagonal GaN is greatly deviated from T_d cubic site symmetry.

4. Comparison with CF analyses of other Ln^{3+} ions doped in GaN

It is interesting and instructive to compare our present CF analysis with those for other Ln^{3+} ($\text{Ln} = \text{Pr, Nd, Sm, Tb}$ and Yb) ions doped in the same host previously reported in Refs. [20–23,25]. All the CF analyses of Ln^{3+} ions in GaN except that for Tb^{3+} ion show Ln^{3+} ions replace the Ga^{3+} sites with C_{3v} symmetry. In other words, most GaN:Ln^{3+} materials have the hexagonal phases. Hereby, our CF comparison is confined to the hexagonal GaN:Ln^{3+} materials.

Two parameters are invoked in our analysis: the scalar CF strength parameter defined by Auzel et al. [28] and the above-defined deviation level from T_d symmetry P of the hexagonal GaN:Ln^{3+} . It is obvious that both these parameters are determined by the CFPs. Nevertheless, the CFPs of the hexagonal GaN:Nd^{3+} have not been provided [21]. Therefore, before making the comparison, we will have to try to extract the CFPs of the hexagonal GaN:Nd^{3+} from the related experimental CF energy levels.

The CF-split energy levels of the relevant manifolds of the hexagonal GaN:Nd^{3+} have been summarized in Table 1 of Ref. [21]. The standard one-electron CF model cannot account for the CF splittings observed within certain multiplets of the $4f^3$ configurations of Nd^{3+} ions [29,30]. For example, the CF splittings of the ${}^2\text{H}(2)_J$ ($J = 9/2$ and $11/2$), ${}^2\text{G}_{7/2}$ and ${}^2\text{F}(2)_J$ ($J = 5/2$ and $7/2$) multiplets are not well explained by the CF fitting calculations [28]. The correlation crystal-field (CCF) techniques [31] can remove these discrepancies between the calculated and observed splittings, but the CCF calculations usually introduce a large number of parameters making the whole calculations more complicated. Here still use the one-electron CF model, but avoid those problematic multiplets. The one-electron CFPs can be obtained by the CF fitting calculations within different 4I_J manifolds, for which the CCF effect is much weaker. According to the above considerations, the observed CF energy levels of the ground ${}^4I_{9/2}$, and excited ${}^4I_{11/2}$, ${}^4I_{13/2}$ and ${}^4F_{3/2}$ multiplets of the hexagonal GaN:Nd^{3+} were chosen to join into the fitting calculations, and listed in Table 3. Following the same fitting procedure with the hexagonal GaN:Er^{3+} , all the fitting parameters were obtained and summarized in Table 3, whereas the calculated energy level values were also collected in Table 5. The present theoretical calculations match well the experimental data, with the standard root-mean-square deviation of 29.5 cm^{-1} .

Table 5
Measured and calculated energy levels (in cm^{-1}) of Nd^{3+} ions in the hexagonal GaN.

Multiplets	Level no.	E_{exp}	E_{calc}	$\Delta = E_{\text{exp}} - E_{\text{calc}}$
$^4I_{9/2}$	1	0	-8.4	8.4
	2	47.6	35.1	12.5
	3	210.5	187.0	23.5
	4	245.2	231.3	13.9
	5	318.6	322.4	-3.8
$^4I_{11/2}$	6	1877.6	1908.0	-30.4
	7	1909.9	1917.0	-7.1
	8	1948.6	1960.8	-12.2
	9	1973.6	2047.6	-74.0
	10	2080.1	2080.3	-0.2
	11	2125.3	2110.1	15.2
$^4I_{13/2}$	12	3848.8	3837.2	11.6
	13	3865.0	3858.6	6.4
	14	3897.2	3878.6	18.6
	15	3921.4	3938.9	-17.5
	16	4040.8	4027.7	13.1
	17	4066.6	4055.6	11.0
	18	4100.5	4088.2	12.3
	$^4I_{15/2}$	19	-	5784.5
20		-	5818.0	-
21		-	5847.0	-
22		-	5886.3	-
23		-	5984.2	-
24		-	6107.1	-
25		-	6167.5	-
26		-	6184.3	-
$^4F_{3/2}$	27	10916.6	10901.5	15.1
	28	10950.5	10967.2	-16.7

Note: The standard deviations of the fitting calculations for the hexagonal GaN: Nd^{3+} is 29.5 cm^{-1} .

To obtain the CF invariant S and the deviation level from T_d symmetry P for the hexagonal GaN: Ln^{3+} ($\text{Ln} = \text{Pr}, \text{Nd}, \text{Sm}$ and Yb), all the related CFPs under point-group basis defined by Eqs. (5a), (5b), (5c) were firstly calculated by applying the Eq. (6) to the original CFPs (defined by Wybourne [13]) listed in Table 3 or Refs. [20,22,25]; then the S_C , S_D , S and P parameters can be obtained and collected in Table 4 with all the CFPs values under point-group basis together.

The results from Table 4 enable comparisons to be made of the S and P parameters along the lanthanide series. Fig. 9 shows the decreasing tendency of the S parameter along the lanthanide series. The best fit using a linear relation has been obtained as follows (in unit of cm^{-1}):

$$S = (2633.70 \pm 353.63) + (-104.61 \pm 43.66)N \quad (8)$$

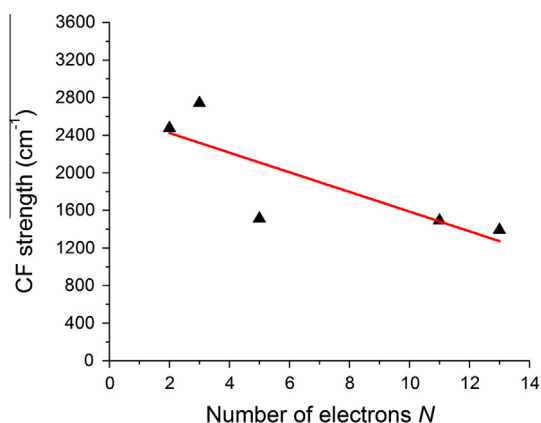


Fig. 9. The variation trend of the CF invariant S against the electron number N of the $4f^N$ configuration in the hexagonal GaN: Ln^{3+} . The linear fitting equation for S is: $2633.70 - 101.61N \text{ cm}^{-1}$.

where N is the number of electrons in the $4f^N$ configuration. This decreasing tendency of the S parameter is in line with the lanthanide contraction effects [32]. The tendency of the P parameter along the lanthanide series is expected to be increasing due to the fact that the distortion of the cluster $[\text{LnN}_4]^{9-}$ gradually becomes small due to the reduction of the ionic radii of the doped Ln^{3+} ions [26]. However, the theoretical calculations show the dependence of the parameter P is decreasing for the first half series and increasing for the second half series. It is known that the different growth and annealing conditions that are used can both probably change the local environment of Ln^{3+} ions in the hexagonal GaN. This might lead to the uncommon dependence of the parameter P along the lanthanide series.

At last, we compared the CF invariant of the cubic GaN: Tb^{3+} with that of Er^{3+} to characterize the CF effects in the cubic GaN. The theoretical calculations employing the definition of CF strength given by Auzel et al. [28] and the CFPs in Table 2 and Ref. [20] show the CF invariants of the cubic GaN respectively doped with Tb^{3+} and Er^{3+} ions are 3109.6 and 974.9 cm^{-1} . The present calculated results similarly suggest the lanthanide contraction effects.

5. Conclusions

Consistent spectroscopic and crystal field studies of the Er^{3+} energy levels in cubic and hexagonal structural modifications of GaN have been performed in the present paper. The experimental data shown here allow us to make a preliminary conclusion about local symmetries of Er^{3+} in both phases of GaN (D_2 and C_{3v} in cubic and hexagonal phase, respectively), where only one emitting center is distinguishable in each phase. The theoretical calculations gave us reliable sets of the crystal field parameters, which allowed for assigning all absorption peaks and getting exact positions of the erbium energy levels. The quality of the crystal field calculations can be judged from a small value of the root mean squared deviation between the theoretical and experimental energy levels (13 cm^{-1}). In addition to the crystal field studies of the erbium levels, we presented the results of the comparative cross-cutting study of the crystal field energy levels of the trivalent lanthanides in hexagonal GaN. In particular, it was found that the crystal field strength is decreasing across the whole lanthanide series, which can be related to the lanthanide contraction and increase of the effective “lanthanide–ligand” chemical bond length.

Acknowledgements

The financial supports by the Estonian Science Foundation Grants Nos. 7456, 6999, 6658, 7612 and GLOFY054MJJD are gratefully acknowledged. C.-G. Ma thanks the financial support of National Natural Science Foundation of China under Grant No. 11204393. M.G. Brik’s research was supported by European Social Fund’s Doctoral Studies and Internationalisation Programme DoRa and European Union through the European Regional Development Fund (Centre of Excellence “Mesosystems: Theory and Applications”, TK114). We would like to thank Prof. M.F. Reid for the use of his suite of software for f-shell system.

Work at TTU is supported by NSF (ECCS-1200168). Jiang and Lin acknowledge the AT&T Foundation for the support of Ed Whitacre and Linda Whitacre endowed chairs.

References

- [1] P.N. Favennec, H. L’Haridon, M. Salvi, D. Moutonnet, Y. Le Guillou, *Electron. Lett.* 25 (1989) 718.
- [2] J.M. Zavada, Dahua Zhang, *Solid-State Electron.* 38 (1995) 1285.
- [3] M.R. Brown, A.F.J. Cox, W.A. Shand, J.M. Williams, *Adv. Quantum Electron.* 2 (1974) 69.

- [4] H. Ennen, J. Schneider, G. Pomrenke, A. Axmann, *Appl. Phys. Lett.* 43 (1983) 943.
- [5] R. Birkhahn, M. Garter, A.J. Steckl, *Appl. Phys. Lett.* 74 (1999) 2161.
- [6] R.G. Wilson, R.N. Schwartz, C.R. Abernathy, S.J. Pearton, N. Newman, M. Rubin, T. Fu, J.M. Zavada, *Appl. Phys. Lett.* 65 (1994) 992.
- [7] C. Ugolini, N. Nepal, J.Y. Lin, H.X. Jiang, J.M. Zavada, *Appl. Phys. Lett.* 89 (2006) 151903.
- [8] Y.N. Xu, W.Y. Ching, *Phys. Rev. B* 48 (1993) 4335.
- [9] A.F. Wright, J.S. Nelson, *Phys. Rev. B* 51 (1995) 7866.
- [10] K. Momma, F. Izumi, *J. Appl. Crystallogr.* 44 (2011) 1272–1276.
- [11] G.K. Liu, in: G.K. Liu, B. Jacquier (Eds.), *Spectroscopic Properties of Rare Earths in Optical Materials*, Tsinghua University Press & Springer-Verlag, Berlin, Heidelberg, 2005, p. 1.
- [12] W.T. Carnall, G.L. Goodman, K. Rajnak, R.S. Rana, *J. Chem. Phys.* 90 (1989) 3443.
- [13] B.G. Wybourne, *Spectroscopic Properties of Rare Earths*, Interscience Publishers, John Wiley & Sons Inc., New York, 1965.
- [14] P. Caro, O. Beaury, E. Antic, *J. Phys. (France)* 37 (1976) 671.
- [15] A. Kozanecki, V. Glukhanyuk, H. Przybylińska, *Phys. Status Sol. (a)* 205 (2008) 38.
- [16] V. Glukhanyuk, H. Przybylińska, A. Kozanecki, *Phys. Status Sol. (c)* 4 (2007) 2605.
- [17] V. Glukhanyuk, H. Przybylińska, A. Kozanecki, W. Jantsch, *Phys. Status Sol. (a)* 201 (2004) 195.
- [18] K. Makarova, M. Stachowicz, V. Glukhanyuk, A. Kozanecki, C. Ugolini, J.Y. Lin, H.X. Jiang, J. Zavada, *Mater. Sci. Eng. B* 146 (2008) 193.
- [19] V. Glukhanyuk, H. Przybylińska, A. Kozanecki, W. Jantsch, *Opt. Mater.* 28 (2006) 746.
- [20] J.B. Gruber, B. Zandi, H.J. Lozykowski, W.M. Jadwisieniczak, I. Brown, *J. Appl. Phys.* 89 (2001) 7973.
- [21] G.D. Metcalfe, E.D. Readinger, H.E. Shen, N.T. Woodward, V. Dierolf, M. Wraback, *J. Appl. Phys.* 105 (2009) 053101.
- [22] J.B. Gruber, B. Zandi, H.J. Lozykowski, W.M. Jadwisieniczak, *J. Appl. Phys.* 91 (2002) 2929.
- [23] J.B. Gruber, B. Zandi, H.J. Lozykowski, W.M. Jadwisieniczak, *J. Appl. Phys.* 92 (2002) 5127.
- [24] R. Maâlej, M. Dammak, S. Kammoun, M. Kammoun, *J. Lumin.* 126 (2007) 695.
- [25] T. Koubaa, M. Dammak, M. Kammoun, W.M. Jadwisieniczak, H.J. Lozykowski, *J. Alloys Compd.* 496 (2010) 56.
- [26] R.D. Shannon, *Acta Crystallogr.* A32 (1976) 751.
- [27] P.H. Butler, *Point Group Symmetry Applications: Methods and Tables*, Plenum Press, New York and London, 1981.
- [28] F. Auzel, O.L. Malta, *J. Phys. (France)* 44 (1983) 201.
- [29] M. Faucher, D. Garcia, P. Caro, J. Derouet, P. Porcher, *J. Phys. (France)* 50 (1989) 219.
- [30] C.L. Li, M.F. Reid, *Phys. Rev. B* 42 (1990) 1903.
- [31] M.F. Reid, D.J. Newman, in: D.J. Newman, Betty Ng (Eds.), *Crystal Field Handbook*, Cambridge University Press, Cambridge, 2000, p. 120.
- [32] F. Auzel, *J. Lumin.* 93 (2001) 129.